Ruthenium-Based Electrocatalysts Supported on Reduced Graphene Oxide for Lithium-Air Batteries

Hun-Gi Jung,[†,§,⊥] Yo Sub Jeong,[†,§] Jin-Bum Park,[†] Yang-Kook Sun,[†,*] Bruno Scrosati,[†,‡,*] and Yun Jung Lee[†,*]

[†]Department of Energy Engineering, Hanyang University, Seoul 133-791, Republic of Korea, and [‡]Department of Chemistry, University of Rome Sapienza, 00185 Rome, Italy. [§]These authors contributed equally to this work. [⊥]Present address: Green City Technology Institute, Korea Institute of Science and Technology, Seoul 136-791, Republic of Korea.

ABSTRACT Ruthenium-based nanomaterials supported on reduced graphene oxide (rGO) have been investigated as air cathodes in non-aqueous electrolyte Li-air cells using a TEGDME-$LiCF_3SO_3$ electrolyte. Homogeneously distributed metallic ruthenium and hydrated ruthenium oxide ($RuO_2 \cdot 0.64H_2O$), deposited exclusively on rGO, have been synthesized with average size below 2.5 nm. The synthesized hybrid materials of Ru-based nanoparticles supported on rGO efficiently functioned as electrocatalysts for Li_2O_2 oxidation reactions, maintaining cycling stability for 30 cycles without sign of TEGDME-$LiCF_3SO_3$ electrolyte decomposition. Specifically, $RuO_2 \cdot 0.64H_2O$-rGO hybrids were superior to Ru-rGO hybrids in catalyzing the OER reaction, significantly reducing the average charge potential to ~3.7 V at the high current density of 500 mA g^{-1} and high specific capacity of 5000 mAh g^{-1}.

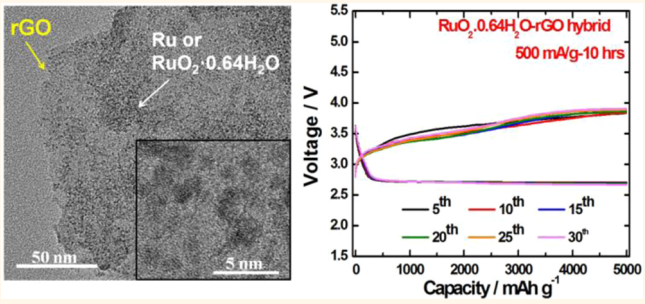

KEYWORDS: reduced graphene oxide · supported catalysts · ruthenium oxide · lithium-air battery · organic electrolyte

Ever-growing demand for renewal in energy sources and for sustainability of the road transport has urged the development of new, high-performance power sources. Among the most promising candidates, lithium-air batteries have recently attracted great interests since, in principle, they offer values of theoretical energy density about 10 times higher than that of any available lithium-ion battery. Even under a prudent perspective, it can be estimated that a Li-air battery may reach a practical specific energy density of ~500 Wh kg^{-1}, a value still considerably higher than the 150 Wh kg^{-1} of the state-of-the-art lithium-ion batteries.[1−4] One of the critical challenges that still prevent the implementation of the Li-air batteries is the slow kinetic of the oxygen reaction resulting in large overpotentials, especially in the anodic oxygen oxidation (OER) direction. Consequently, novel electrocatalysts for smoothing out OER are extensively searched worldwide. Although the real effectiveness of the catalytic activity is still under debate,[5,6] recent studies showed that the oxygen reduction reaction (ORR) is rather insensitive to the presence of catalysts, such as transition metal oxide (Co_3O_4,[7] MnO_2[8]) or even noble metals[9−11] since the reaction is satisfactorily promoted by the carbon support alone. Different is the situation related to the oxygen evolution reaction (OER) that appears catalytically sensitive.[10] There are, however, chances that the catalytic action rather than the desired oxidation of Li_2O_2 may in fact promote the decomposition of weak electrolytes, such as those based on organic carbonate[12] or dimethyl ether (DME)[6] solutions. Therefore, the choice of stable and robust salt−electrolyte systems, such as that provided by $LiCF_3SO_3$-tetra(ethylene glycol) dimethyl ether (TEGDME) electrolytes,[13,14] is a prerequisite for carrying out a valid screening of catalysts for Li-air rechargeable batteries.

Carbon-supported noble metals have been widely investigated as electrocatalysts, and the literature results demonstrate that the control of the nanostructures of the catalyst−support hybrid is a factor of key importance.[15,16] In this respect, the use of a

* Address correspondence to yksun@hanyang.ac.kr, bruno.scrosati@uniroma1.it, yjlee94@hanyang.ac.kr.

Received for review January 29, 2013 and accepted March 29, 2013.

Published online March 29, 2013
10.1021/nn400477d

two-dimensional graphene support has been proven to be quite effective in enhancing catalytic activity compared to conventional carbon supports, such as Vulcan[15] or carbon black.[16] The favorable behavior of the graphene supports may be attributed to a series of positive features, such as (i) a high dispersion and low aggregation[15] of noble metal catalysts resulting from an enhanced interaction between functionalized graphene surface and the noble metals[17] and (ii) a large surface area of the graphene support.[18]

Ruthenium-based nanoparticles such as metallic Ru and RuO_2, hydrated or anhydrous, have been actively explored as catalysts in various chemical and electrochemical oxidation reactions such as alcohol oxidation,[19,20] amine oxidation,[21] CO oxidation,[22,23] and water electrolysis or water splitting oxygen evolution reaction.[24−28] Recently, Shao-Horn *et al.*,[29] by observing the potentiostatic oxidation current of chemically synthesized Li_2O_2/Ru supported on Vulcan carbon composites, also demonstrated that Ru nanoparticles could significantly increase the kinetics of oxygen oxidation in carbonate-free, 1,2-dimethoxyethane, DME-based electrolytes. The level of the catalytic activity varied depending upon the given reaction mechanisms. For instance, in cases of alcohol, amine, and CO oxidation processes, RuO_2 showed better catalytic activity than metallic Ru. In OER of water oxidation in acidic aqueous systems, RuO_2 has been proven to be the best catalyst with sufficient stability since metallic Ru shows similar[30] or inferior catalytic activity[31] but heavily corrodes.[26] Shao-Horn and coworkers[32] recently confirmed the catalytic activity of RuO_2 for oxygen evolution in acid and alkaline aqueous solutions, also showing that its stability under OER conditions is higher than that of Ru metal−carbon composites. Finally, Oh and Nazar[33] have reported a study on the electrochemical properties of bismuth and lead ruthenate pyrochlores supported on carbon as catalysts for oxygen reaction in Li/O_2 cells with a $LiPF_6$-TEGDME electrolyte. To the best of our knowledge, however, there are no previous reports on the oxygen-involving reactions catalyzed by Ru-based hybrids supported on functionalized graphene in Li/O_2 cells using a $LiCF_3SO_3$-TEGDME electrolyte.

In this work, we evaluate the electrocatalytic activity of ruthenium-based nanomaterials loaded on reduced graphene oxide (rGO) for promoting the OER in nonaqueous, Li-oxygen cells using a $LiCF_3SO_3$-TEGDME solution as the preferred electrolyte. We demonstrate that our nanohybrid structures, benefitting by the unique combination of a porous rGO support with Ru-based hybrid nanocrystals, decrease the value of the charging overpotential compared to that resulting from the use of conventional, carbon-based, catalyst-free electrodes. We show that in Li/O_2 cells using electrodes loaded by Ru-based rGO-supported hybrid catalysts, the OER reaction proceeds with an average charging potential of ∼3.7 V even under highly demanding conditions, such as those associated with a high current density (*i.e.*, 500 mA g^{-1}) and a high capacity (*i.e.*, 5000 mAh g^{-1}). No electrolyte decomposition was observed, and the cell shows stable cycling performances for over 30 cycles.

RESULTS AND DISCUSSION

In this research, we have examined the catalytic activity of three main materials, namely, (i) reduced graphene oxide; (ii) ruthenium metal supported on graphene, hereafter simply referred as Ru-rGO hybrid; and (iii) hydrated ruthenium oxide supported on graphene, hereafter simply referred as $RuO_2 \cdot H_2O$-rGO hybrid. The X-ray diffraction (XRD) patterns of the two hybrids confirm the presence of nanocrystalline metallic Ru and rutile RuO_2 along with the rGO in the Ru-rGO and $RuO_2 \cdot H_2O$-rGO hybrids, respectively (see Supporting Information Figure S1). The structural water content in rGO-supported hydrated $RuO_2 \cdot H_2O$ particles was estimated using thermogravimetric analysis (TGA) obtaining a total weight loss of $RuO_2 \cdot H_2O$ of ∼8 wt % corresponding to a $RuO_2 \cdot 0.64H_2O$ composition (Figure S2b). TGA was also used to determine the catalyst loading on rGO that was 44 wt % Ru-rGO and 55 wt % $RuO_2 \cdot 0.64H_2O$-rGO (Figure S2a,c). The carbon in Ru-based rGO hybrids decomposed at lower temperatures than graphitic carbon or rGO-only,[34] probably due to the interaction between noble metal nanoparticles and graphene carbon that might influence the bond strength between the backbones or even favor its catalytic decomposition. Finally, the Ru-rGO and $RuO_2 \cdot 0.64H_2O$-rGO hybrids used in this work were characterized by X-ray photoelectron spectroscopy (XPS) (Figure S3).

Figure 1 reports the scanning electron microscopy (SEM) and transmission electron microscopy (TEM) microstructural analyses of Ru-rGO and $RuO_2 \cdot 0.64H_2O$-rGO hybrids. The SEM images in Figure 1a,d evidence the wrinkled, porous two-dimensional rGO morphology, forming featured porous 3-D networks of the rGO platform. The presence of carbon, ruthenium, and oxygen was verified by the energy-dispersive X-ray spectroscopy (EDX) images shown in the insets of the figures. The TEM images of Figure 1b,e reveal the intimate hybrid structure of the rGO-supported catalysts: Ru and $RuO_2 \cdot 0.64H_2O$ nanoparticles are exclusively deposited on rGO and distributed homogeneously across its surface. It is worth noting that effective catalytic activity is expected to be associated with high surface area of the active catalytic sites, as in fact provided here by the well-separated nanoparticles of Ru and $RuO_2 \cdot 0.64H_2O$. The high-magnification HRTEM images reported in the insets of Figure 1b,e evidence the crystalline nature of these nanoparticles. Finally, the HRTEM analysis allowed us to also determine the particle size distribution of the Ru and $RuO_2 \cdot 0.64H_2O$

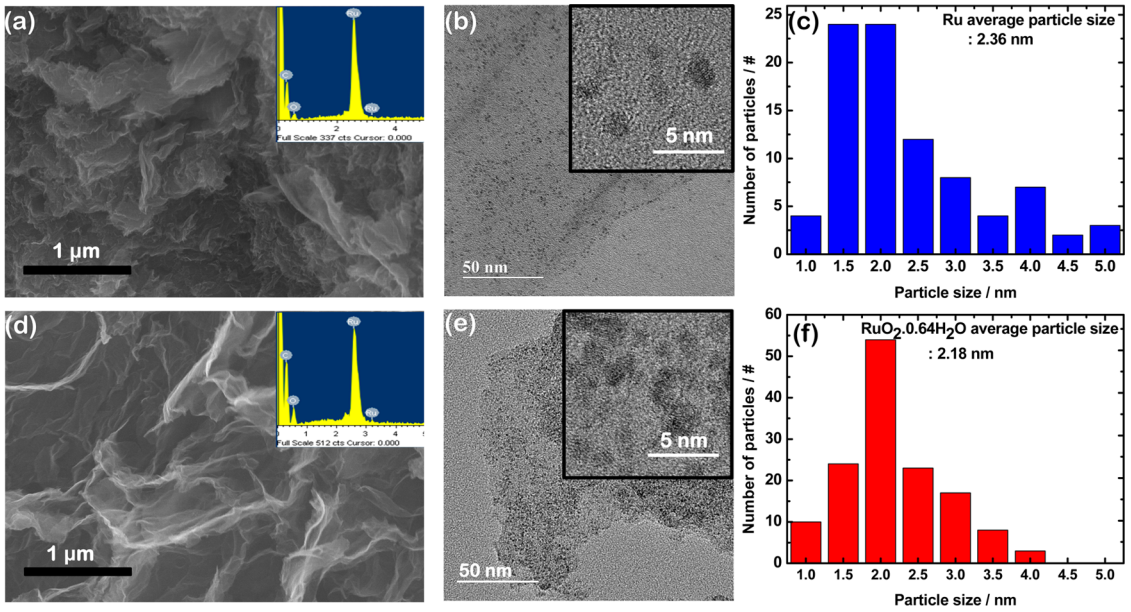

Figure 1. Microstructural analysis of Ru-rGO and $RuO_2 \cdot 0.64H_2O$-rGO hybrids: (a) SEM image of porous Ru-rGO hybrid; (inset) SEM-EDX of Ru-rGO hybrid; (b) TEM images of Ru-rGO hybrid (inset: HRTEM image); (c) particle size distribution of Ru-rGO hybrid; (d) SEM image of porous $RuO_2 \cdot 0.64H_2O$-rGO hybrid; (inset) SEM-EDX of $RuO_2 \cdot 0.64H_2O$-rGO hybrid; (e) TEM images of $RuO_2 \cdot 0.64H_2O$-rGO hybrid (inset: HRTEM); and (f) particle size distribution of $RuO_2 \cdot 0.64H_2O$-rGO hybrid.

powders, as reported in Figure 1c,f: for both systems, most particles fall within the size range of 1−4 nm, with an average size of 2.36 and 2.18 nm for Ru and $RuO_2 \cdot 0.64H_2O$, respectively. The Brunauer−Emmett−Teller (BET) specific surface areas of rGO-only powder, Ru-rGO hybrid, and $RuO_2 \cdot 0.64H_2O$-rGO hybrid are 51.7, 124.0, and 174.5 $m^2\ g^{-1}$, respectively. The pore volume is 0.049, 0.184, and 0.197 $cm^3\ g^{-1}$ for rGO-only powder, Ru-rGO hybrid, and $RuO_2 \cdot 0.64H_2O$-rGO hybrid, respectively. The surface area of the rGO-only powder, due to the restacking of rGO sheets during the drying process from colloidal rGO, has a similar value of that of Super P carbon, estimated as 61.1 $m^2\ g^{-1}$. The surface area of rGO-supported catalysts, however, is much higher since the presence of the catalysts on rGO effectively suppressed the restacking of the rGO sheets. It is expected that the increased surface area and pore volume could contribute to enhance the reversible capacity of the oxygen electrode by facilitating the transport of O_2 gas and Li^+ ions and accommodating the solid discharge product. This work, however, mainly focuses on the investigation of the catalytic performance of the Ru-based materials to address the overpotential issues of the OER reaction in Li−O_2 cells, and in this regard, the small particle size and well-separated uniform distribution of the catalysts on the conducting support in our hybrid system are certainly important features.

To confirm this expectation, we first assumed that the porous rGO, in view of its general high surface area, could provide preferential reaction sites for O_2 gas, Li^+ ions, and electrons, thus being itself a promising electrode for the oxygen process.[35] Indeed, the surface functional groups and defects, as those occurring in rGO, have been reported to catalyze oxygen-involving reactions in aqueous electrolytes[16] as well as in alkyl carbonate electrolyte[36] Li−O_2 cells, where the main discharge product is OH^- for the former and Li_2CO_3 for the latter. However, as revealed by the BET analysis, rGO-only powder showed similar specific surface area than that of Super P carbon, with this effectively precluding the beneficial role of a higher surface area. Accordingly, we could not detect any specific catalytic effect for both ORR (discharge process) and OER (charge process) compared to Super P in the case where a cathode using rGO-only was applied in our $LiCF_3SO_3$-TEGDME electrolyte-based Li/O_2 cell (see Figure S4) so as to lead us to the conclusion that, unlike the aqueous electrolyte and carbonate electrolyte systems, the functional groups and defects on the rGO surface do not enhance the Li_2O_2 formation−oxidation reaction any better than the common Super P carbon substrate.

On the contrary, rGO-supported Ru and $RuO_2 \cdot 0.64H_2O$ catalysts showed quite a different behavior. Figure 2 illustrates the discharge (ORR)−charge (OER) voltage profiles of Li/O_2 coin-type cells using electrodes based on pristine rGO, Ru-rGO, and $RuO_2 \cdot 0.64H_2O$-rGO hybrids. The cells were cycled under the capacity-controlled regimes of 2000 and of 5000 mAh g^{-1}, and Figure 2a,d compares the voltage profiles of their respective fifth cycle. Variations of the voltage profile during the first five cycles (from first to fifth cycle) are provided in Figure S5. While the charge potential was rather fluctuating for the rGO-only electrode, Ru-based hybrid electrodes showed stable OER potentials after the

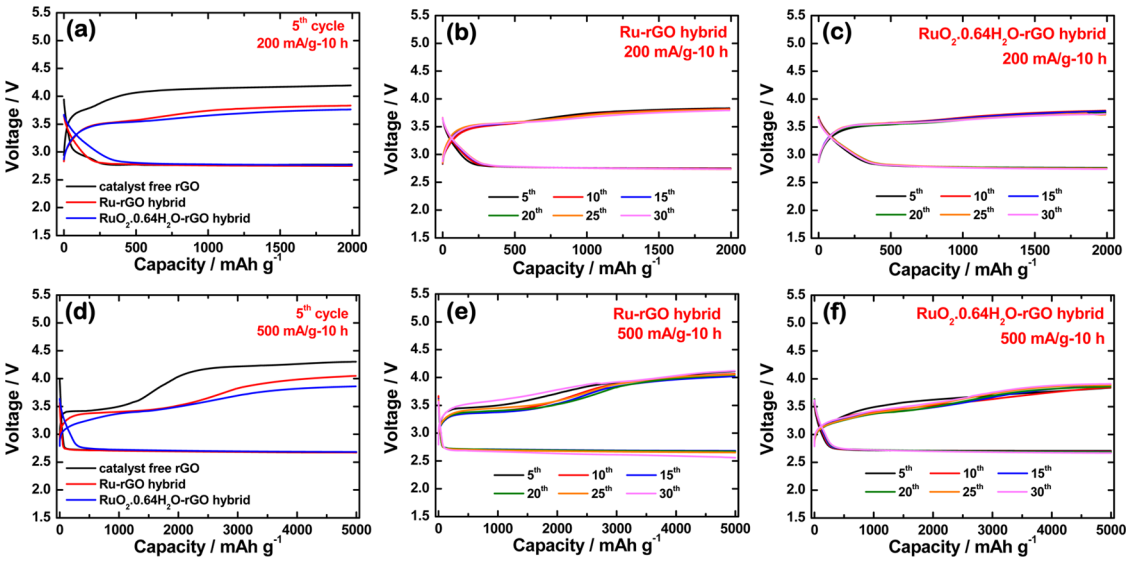

Figure 2. Discharge–charge cycles of Li-air cells using rGO, Ru-rGO hybrid, and $RuO_2 \cdot 0.64H_2O$-rGO hybrid under various specific capacity limits. (a–c) Current = 200 mA g^{-1}; time = 10 h; cycling capacity = 2000 mAh g^{-1}; voltage profiles of (a) fifth cycle and following cycles of (b) Ru-rGO hybrid and (c) $RuO_2 \cdot 0.64H_2O$-rGO hybrid. (d–f) Current = 500 mA g^{-1}; time = 10 h; cycling capacity = 5000 mAh g^{-1}; voltage profiles of (d) fifth cycle and following cycles of (e) Ru-rGO hybrid and (f) $RuO_2 \cdot 0.64H_2O$-rGO hybrid. The capacity was normalized by the total weight of oxygen electrodes (rGO or rGO + catalyst).

third cycle. Clearly, the cells using electrodes with the Ru-based rGO hybrids display a significant reduction in charge potentials, passing from ~4.3 V for rGO to ~3.9 V for the Ru-rGO hybrid and ~3.7 V for the $RuO_2 \cdot 0.64H_2O$-rGO hybrid, even under the high capacity regime of 5000 mAh g^{-1}; in contrast, their discharge potentials did not substantially differ. The latter result is in line with the generally accepted assumption that the ORR Li_2O_2 formation reaction is hardly affected by catalysts which instead are of importance for enhancing the kinetics of the OER Li_2O_2 reconversion. The origin of the two plateaus in the charge potential profile is not clear at this moment. We speculate that it might be associated with decomposing Li_2O_2 products with different electrochemical reactivity. Our previous report,[14] showing that in the discharge product figure both spherical amorphous, hollow amorphous and crystalline Li_2O_2 that in turn might have different electrochemical activity upon decomposition, partially supports this hypothesis. Further investigation, however, is certainly needed to reach a final explanation of the double-plateau trend.

Notice that the OER potential did not change dramatically in Li/O_2 cells using $RuO_2 \cdot 0.64H_2O$-rGO hybrid electrodes when the discharge and charge current was increased from 200 mA g^{-1} to 500 mAh g^{-1} (compare Figure 2c,f). McCloskey *et al.*,[37] by studying the $^{18}O_2$ oxidation process, determined that the highest oxygen evolution rate occurs in the voltage region extending from 3.1 to 4.0 V, remaining then low up to the onset of electrolyte decomposition, that is, above 4.5 V. Since the charging potential of our Li/O_2 cells using $RuO_2 \cdot 0.64H_2O$-rGO hybrid electrodes entirely evolves in the voltage region below 4.0 V (see Figure 2a,c,d,f),

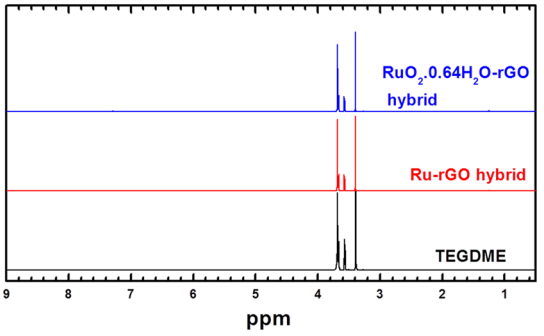

Figure 3. Comparison of ^1H NMR spectra obtained for a TEGDME electrolyte of Li-air cells using rGO, Ru-rGO hybrid, and $RuO_2 \cdot 0.64H_2O$-rGO hybrid after cycling test (capacity = 5000 mAh g^{-1}).

we can expect that the kinetics of the O_2 evolution reaction would be fast during the whole charge process, with this finally accounting for the very good rate capability displayed in these cells. Also the charge–discharge energy efficiency increased considerably when passing from cells using cathodes based on rGO-only to those using the $RuO_2 \cdot 0.64H_2O$-rGO hybrid, namely, from 66 to 75%. Finally, even after 30 cycles at capacity regimes of 2000 mAh g^{-1} (see Figure 2b,c) and 5000 mAh g^{-1} (see Figure 2e,f), the response of cells using the Ru-based hybrid catalyst remained very stable with no evidence of TEGDME-$LiCF_3SO_3$ electrolyte decomposition, as confirmed by ^1H nuclear magnetic resonance (NMR) analysis (see Figure 3).

Figure S6 shows that $Li–O_2$ cells employing Ru-based hybrid electrodes started to degrade after 35 cycles. Also, a cell using $RuO_2 \cdot 0.64H_2O$-rGO hybrid cathodes, when cycled in a voltage window extending

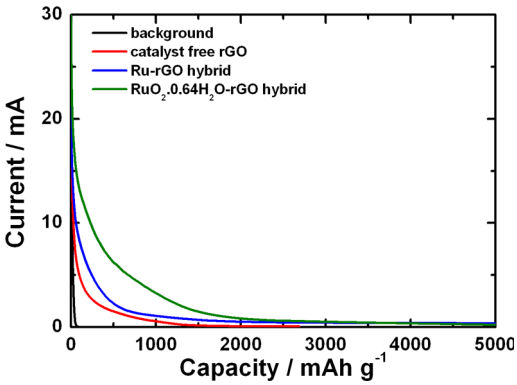

Figure 4. Potential step chronoamperometry for the discharged electrodes in Li−O_2 cells. The cell was first discharged at 500 mA g^{-1} for 10 h to give discharge capacity of 5000 mAh g^{-1}. After discharge, the cell potential was held at 2.9 V for 3 h. Then the potential was stepped from 2.9 to 4.0 V *vs* Li/Li^+.

from 2.0 to ~4.3 V, showed a rapid capacity decay. We believe that this apparent poor cyclability is not merely associated with the degradation (including pore blocking) of the air cathode but rather to a progressive degradation of the Li-metal anode. It has been, in fact, shown that Li-metal anode, if not adequately protected, may severely corrode upon cycling.[38] In addition, it is important to point out that, in order to obtain high reversibility, it is advisable to limit the discharge process of Li−O_2 cells to the formation of Li_2O_2. We have, in fact, shown that the reversibility is seriously affected if the process is extended to Li_2O since this condition prevents full reconversion to Li and O_2.[39]

To further compare the catalytic activity of Ru-based hybrid catalysts with that of rGO-only on OER kinetics, three related fully discharged cells were potentiostatically recharged at 4 V, and the resulting chronoamperometric curves are shown in Figure 4. The trends demonstrate that the current level in the cell with the hybrid catalysts, especially with the $RuO_2 \cdot 0.64H_2O$-rGO hybrid, is consistently higher than that using pristine rGO, this again confirming the superior activity of the former. The question that can be raised here is if the electrocatalysts employed actually catalyze the reversible Li_2O_2 formation−reconversion reaction and not undesirable side reactions, such as that between Li_2O_2 and carbon.

The electrolyte stability under the presence of Ru-based hybrid catalysts was already demonstrated by the NMR analysis reported in Figure 3. We confirm the absence of side reactions at the electrode side by the XPS chemical attribute analysis reported in Figure 5. The spectra clearly reveal that the main discharge product for the $RuO_2 \cdot 0.64H_2O$-rGO hybrid electrode was Li_2O_2 and that it decomposed completely upon charging (Figure 5a). Admittedly, a small amount of Li_2CO_3 was observed after charging; we believe, however, that it originates from the oxygen functionalities of the rGO support (compare Figure 5b,c). The surface oxygen functional groups of rGO could, in fact, react with lithium with an initial formation of Li_2CO_3; however, since they are present in a very limited amount, this process is not expected to significantly affect the overall performance or reversibility of the electrochemical reaction, as indeed demonstrated by the excellent cycling reversibility shown by the Ru-based rGO hybrid air cathodes tested in this work. The same result was found for the Ru-rGO hybrid.[40] All included, we concluded that Ru-based electrocatalysts truly catalyze the reversible Li_2O_2 formation−reconversion reaction.

In our assessment for the catalyzed Li_2O_2 oxidation (charging) process, we found that $RuO_2 \cdot H_2O$ behaves better than Ru (see Figure 2). The exact explanation for the high catalytic activity of $RuO_2 \cdot H_2O$ on the OER in non-aqueous Li/O_2 cells is not yet totally clear to us. At this stage, we may only speculate that this activity may closely depend upon the mechanism of the Li_2O_2 reconversion reaction and of its intermediates. For instance, in the case of chemical oxidation of CO, the catalytic activity is determined by the interplay of the surface adsorption energy of molecular oxygen and its dissociation probability. For assuring optimum catalytic activity, the dissociation probability should not be too low and the adsorption energy not too high. Due to its very strong oxygen binding that limits the supply of active oxygen species, metallic Ru is a poor catalyst for CO oxidation. On the contrary, RuO_2 is much more active due to the weaker oxygen bonding compared to chemisorbed oxygen on metallic Ru.[22] It has been shown that electrocatalyzed OER in acidic aqueous systems involves surface-adsorbed O, OH, and OOH intermediates,[31,41] and for both metallic Ru and RuO_2-catalyzed processes, the rate-limiting step is the formation of OOH intermediates. It has also been reported that RuO_2 catalysts showed lower OER overpotentials than metals, mainly due to oxygen binding and hydroxyl binding surface forces.[31]

It is apparent that the OER in non-aqueous electrolyte Li−O_2 cells follows a different reaction pathway from ORR[42] and that the direct reconversion of Li_2O_2 to Li^+ and O_2 does occur without formation of LiO_2 intermediates in the course of the noncatalyzed oxidation of Li_2O_2 while the formation of these intermediates has been verified for the opposite ORR.[39,42] In view of the above considerations, we may explain the better performance of RuO_2 in the above-mentioned catalyzed Li_2O_2 reconversion reaction by speculating that its mechanism is closely associated with the surface-adsorbed oxygen intermediates and, consequently, that the binding energy of the oxygen atoms could be a key parameter for influencing the activity of the catalyst itself. Even assuming the same activity per site for metallic Ru and for $RuO_2 \cdot H_2O$, the latter is expected to operate with a higher efficiency since the density of Ru is 10.65 g cm^{-3} while that of $RuO_2 \cdot H_2O$ is almost half, 6.97 g cm^{-3}. In our study, Ru and $RuO_2 \cdot 0.64H_2O$ have similar particle size (see Figure 1); hence, by using

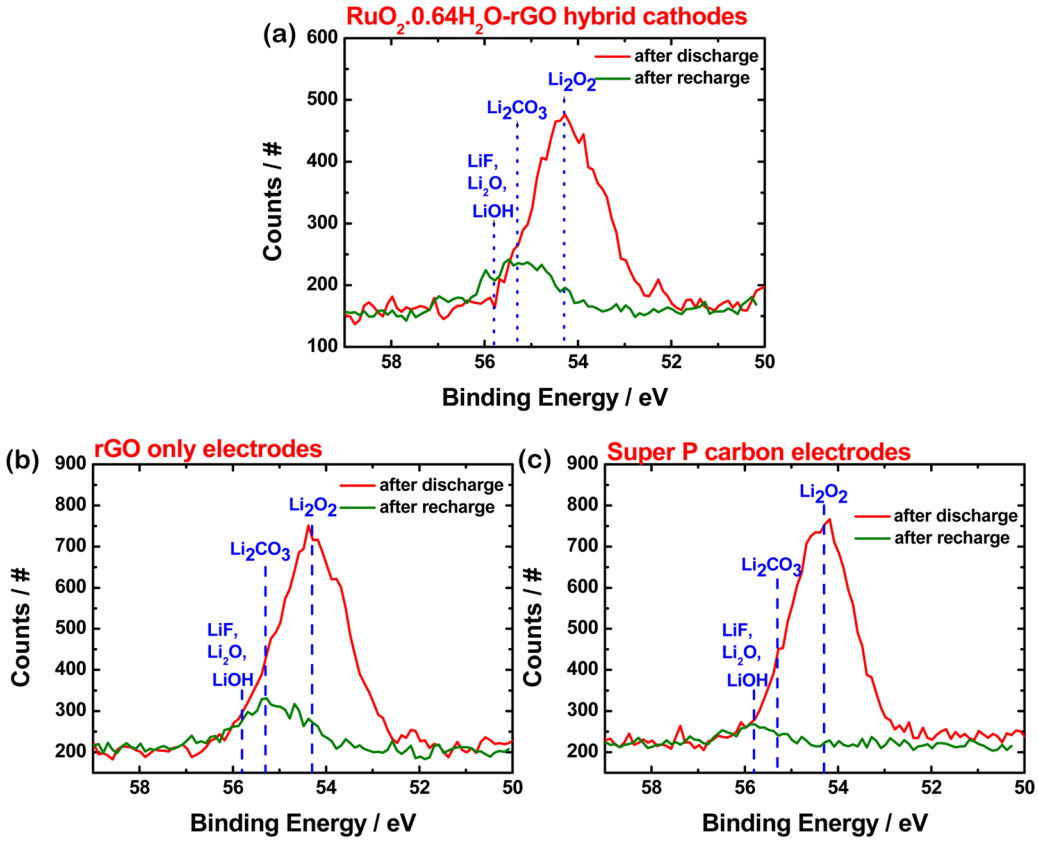

Figure 5. XPS Li 1s peaks of the discharged and recharged electrodes using (a) $RuO_2 \cdot 0.64H_2O$-rGO hybrid, (b) rGO-only, and (c) Super P carbon.

the same catalyst mass loading onto rGO, the number of active surface sites is expected to be higher for $RuO_2 \cdot 0.64H_2O$, as effectively apparent by comparing of Figure 1e with Figure 1b. Additional work is certainly needed to confirm this interpretation; this work is, in fact, in progress in our laboratories.

Finally, we address the stability aspect in respect to the Ru-based nanomaterials tested in this study. Since RuO_2 is hydrated, the incorporated water molecule might, in principle, cause side reactions, such as LiOH formation. The H_2O in hydrated RuO_2, however, is not surface-adsorbed but rather a structural water included in the molecular structure, and in this feature, it is not expected to easily decompose. In fact, we did not detect any evidence of LiOH by XPS analysis of discharged $RuO_2 \cdot 0.64H_2O$-rGO hybrid electrodes. Furthermore, the cycling data presented in this work showed stable retention up to 35 cycles, finally confirming the stability of H_2O in hydrated RuO_2. We also measured the time evolution of the open circuit voltage (OCV) of the cells with rGO-only and $RuO_2 \cdot 0.64H_2O$-rGO hybrid cathodes since an eventual change in OCV would, in fact, show the occurrence of side processes. However, no change over time was detected. Electrochemical impedance spectroscopy (EIS) was also employed to monitor impedance change over time; also this test did not evidence the occurrence of any unexpected reaction since the impedance for the cells with rGO-only and with $RuO_2 \cdot 0.64H_2O$-rGO hybrid cathodes was quite stable. Therefore, we can reasonably conclude that the incorporated water molecules are not involved in the electrochemical reaction. This point is further discussed in the Supporting Information; see Figure S7.

CONCLUSION

Ru-based nanomaterials supported on rGO have been tested as catalysts for the oxygen reduction (ORR, Li_2O_2 formation) and oxidation (OER, Li_2O_2 reconversion) in the Li/O_2 cells using a TEGDME-$LiCF_3SO_3$ electrolyte. The results demonstrate that, while rGO itself cannot boost Li_2O_2 formation and oxidation reaction any better than common Super P carbon, Ru-based nanoparticles have instead a definite ability to catalyze OER with fast kinetics and no electrolyte decomposition. In particular, we show that hybrids based on hydrated ruthenium oxide supported on graphene ($RuO_2 \cdot 0.64H_2O$-rGO) outperformed those based on metal ruthenium also supported on graphene (Ru-rGO) by a superior catalytic activity, remarkably reducing charge potentials to ~3.7 V even at high current density of 500 mA g^{-1} and high capacity of 5000 mAh g^{-1}. We show that Li-air cells employing $RuO_2 \cdot 0.64H_2O$-rGO cathodes maintained stable

cycling performances for over 30 cycles. We believe that this work may contribute to enhance the energy power performances of the Li-air cells by demonstrating the key role of proper engineering of the catalyst materials and nanostructures.

Some concern may arise on the crystallinity of our Ru-based materials since the peaks shown in Figure S1 are not totally well-defined. This apparent lack of crystallinity might be related to the nanosize dimension of the electrocatalysts employed here. Highly crystalline catalysts, usually prepared at high temperature, show better stability than amorphous but have lower overall catalytic activity.[24] We show here that our Ru-based materials promote stable cycling for more than 30 cycles (see later); however, admittedly this is not conclusive evidence in terms of prolonged operation. However, at the present status of this study, we cannot undertake long-term evaluation of the cells due to a series of still unsolved issues, including the degradation of the Li-metal anode, pore clogging, and many other problems related with cell components. Therefore, we plan to evaluate the long-term stability once a stable cell configuration is determined. This work is in progress in our laboratories.

METHODS

Material Synthesis. Graphene oxide (GO) was prepared by modified Hummers method.[43,44] Ru-rGO hybrid was synthesized by modified polyol method.[45] A 100 mL GO dispersion (1 mg mL^{-1}) in ethylene glycol (EG) was first prepared with the aid of horn sonication for 1 h, then added by 10 mL of $RuCl_3$ solution dissolved in EG (21 mg mL^{-1}) and incubated for 2 h. The pH of the solution was adjusted to 13 with NaOH (2.5 M in EG). The reaction temperature was increased to 120 °C, and upon reaching 120 °C, and a solution of $NaBH_4$ reducing agent dissolved in EG was slowly injected. The so obtained solution was refluxed at this temperature for 1 h and then cooled to room temperature. The final rGO-supported metallic Ru product was filtered, washed, and dried under vacuum. The $RuO_2 \cdot 0.64H_2O$-rGO hybrid was synthesized by a mild hydrothermal reaction.[46,47] An ultrasonicated, aqueous GO dispersion (0.67 mg mL^{-1}) was mixed with 30 mg of $RuCl_3$. After 30 min of incubation, the resulting solution was transferred to the Teflon-lined autoclave and reacted hydrothermally at 180 °C for 12 h. The precipitation was filtered, washed, and dried.

Characterization. The microstructure of supported catalysts was analyzed by X-ray diffraction (XRD, Rigaku D/Max-2500 powder diffractometer with Cu Kα radiation), transmission electron microscopy (JEOL JEM-2100F), and scanning electron microscopy (Hitachi S-4800). The catalyst composition was determined by thermogravimetric analysis carried out using a Netzsch TG209F3 apparatus at a heating rate of 10 °C min^{-1} in air flow. Nitrogen sorption measurements were performed using Autosorb-IQ MP (Quantachrome Inc.) at 77 K, and specific surface area was calculated using the Brunauer–Emmett–Teller method. Before measurement, the sample was outgassed under vacuum at 100 °C for 3 h. XPS was measured on ThermoVG K-alpha. Finally, the electrolyte stability was determined by ^1H NMR analysis, conducted in $DCCl_3$ (chloroform-d_6) as solvent, and tetramethylsilane (TMS) as a reference using a VNMRS 600 MHz instrument. For this test, the electrolyte was extracted from disassembled tested cells in an argon-filled glovebox.

Electrochemical Test. For the preparation of the oxygen electrodes to be tested in Li/O_2 cells, rGO, Ru-rGO hybrid, and $RuO_2 \cdot 0.64H_2O$-rGO hybrid were intimately mixed in a *N*-methyl-2-pyrrolidone (NMP) solution and a polyvinylidene fluoride binder (PVDF) with a weight ratio of 8:2. The so obtained slurry was coated on a gas diffusion layer (TGP-H-030 carbon paper, Torray) with a loading density of 1.0 ± 0.1 mg_{carbon} cm^{-2} and dried for 12 h at 100 °C under vacuum to remove the residual solvent. $Li-O_2$, R2032 coin-type cells were assembled in an argon-filled glovebox (MBRAUN, H_2O < 0.1 ppm, O_2 < 0.1 ppm). The positive top cover was machine-drilled to evenly distribute 21 × 1.0 mm diameter holes for the oxygen intake. The cell consisted of metallic lithium foil anode (400 μm thick), the aforementioned carbon cathode, and glass fiber (Whatman) separator. A solution of $LiCF_3SO_3$ (Aldrich) in a tetra(ethylene glycol) dimethyl ether (TEGDME) solvent with a molar ratio of 1:4 was used as the electrolyte. All solvents were also dried for several days over activated molecular sieves prior to use to reduce the moisture content below 10 ppm, as determined by Mettler-Toledo Karl Fischer. The $Li-O_2$ cells were electrochemically tested by using galvanostatic cycling with a VMP3 biologic instrument on time-controlled mode at a curnet density of 200 and 500 mA g^{-1} for 10 h. For these tests, the cell was placed in an oxygen-filled chamber with a pressure slightly higher than 1 atm.

Conflict of Interest: The authors declare no competing financial interest.

Acknowledgment. This work was supported by the Human Resources Development Program (No. 20124010203310) of the Korea Institute of Energy Technology Evaluation and Planning (KETEP) grant funded by the Korea government Ministry of Knowledge Economy. This research was also supported by Basic Science Research Program through the National Research Foundation of Korea (NRF) funded by the Ministry of Education, Science and Technology (Grant No. 2012R1A1A1009029).

Supporting Information Available: XRD, TGA of hybrid catalysts; XPS of GO and hybrid catalysts; first cycle charge–discharge curves of lithium-air cells using rGO-only and Super P carbon; electrochemical properties of lithium-air cells for the first five cycles; ^1H NMR spectra obtained for a TEGDME electrolyte of Li-air cells after cycling test; cycling profile of the Li-air cells employing hybrid catalysts up to 35 cycles under capacity limited condition of 2000 mAh g^{-1}. This material is available free of charge *via* the Internet at http://pubs.acs.org.

REFERENCES AND NOTES

1. Bruce, P. G.; Freunberger, S. A.; Hardwick, L. J.; Tarascon, J.-M. Li-O_2 and Li-S Batteries with High Energy Storage. *Nat. Mater.* **2012**, *11*, 19–29.
2. Christensen, J.; Albertus, P.; Sanchez-Carrera, R. S.; Lohmann, T.; Kozinsky, B.; Liedtke, R.; Ahmed, J.; Kojic, A. A Critical Review of Li/Air Batteries. *J. Electrochem. Soc.* **2012**, *159*, R1–R30.
3. Scrosati, B.; Garche, J. Lithium Batteries: Status, Prospects and Future. *J. Power Sources* **2010**, *195*, 2419–2430.
4. Scrosati, B.; Hassoun, J.; Sun, Y. K. Lithium-Ion Batteries. A Look into the Future. *Energy Environ. Sci.* **2011**, *4*, 3287–3295.
5. Shao, Y.; Park, S.; Xiao, J.; Zhang, J.-G.; Wang, Y.; Liu, J. Electrocatalysts for Nonaqueous Lithium-Air Batteries: Status, Challenges, and Perspective. *ACS Catal.* **2012**, *2*, 844–857.
6. McCloskey, B. D.; Scheffler, R.; Speidel, A.; Bethune, D. S.; Shelby, R. M.; Luntz, A. C. On the Efficacy of Electrocatalysis in Nonaqueous Li-O_2 Batteries. *J. Am. Chem. Soc.* **2011**, *133*, 18038–18041.
7. Debart, A.; Bao, J.; Armstrong, G.; Bruce, P. G. An O_2 Cathode for Rechargeable Lithium Batteries: The Effect of a Catalyst. *J. Power Sources* **2007**, *174*, 1177–1182.
8. Debart, A.; Paterson, A. J.; Bao, J.; Bruce, P. G. α-MnO_2 Nanowires: A Catalyst for the O_2 Electrode in Rechargeable

Lithium Batteries. *Angew. Chem., Int. Ed.* **2008**, *47*, 4521–4524.
9. Lu, Y.-C.; Gasteiger, H. A.; Crumlin, E.; McGuire, R., Jr.; Shao-Horn, Y. Electrocatalytic Activity Studies of Select Metal Surfaces and Implications in Li-Air Batteries. *J. Electrochem. Soc.* **2010**, *157*, A1016–A1025.
10. Lu, Y.-C.; Gasteiger, H. A.; Parent, M. C.; Chiloyan, V.; Shao-Horn, Y. The Influence of Catalysts on Discharge and Charge Voltages of Rechargeable Li-Oxygen Batteries. *Electrochem. Solid State Lett.* **2010**, *13*, A69–A72.
11. Lu, Y.-C.; Xu, Z.; Gasteiger, H. A.; Chen, S.; Hamad-Schifferli, K.; Shao-Horn, Y. Platinum-Gold Nanoparticles: A Highly Active Bifunctional Electrocatalyst for Rechargeable Lithium-Air Batteries. *J. Am. Chem. Soc.* **2010**, *132*, 12170–12171.
12. Freunberger, S. A.; Chen, Y.; Peng, Z.; Griffin, J. M.; Hardwick, L. J.; Barde, F.; Novak, P.; Bruce, P. G. Reactions in the Rechargeable Lithium-O_2 Battery with Alkyl Carbonate Electrolytes. *J. Am. Chem. Soc.* **2011**, *133*, 8040–8047.
13. Jung, H. G.; Hassoun, J.; Park, J. B.; Sun, Y. K.; Scrosati, B. An Improved High-Performance Lithium-Air Battery. *Nat. Chem.* **2012**, *4*, 579–585.
14. Jung, H. G.; Kim, H. S.; Park, J. B.; Oh, I. H.; Hassoun, J.; Yoon, C. S.; Scrosati, B.; Sun, Y. K. A Transmission Electron Microscopy Study of the Electrochemical Process of Lithium-Oxygen Cells. *Nano Lett.* **2012**, *12*, 4333–4335.
15. Kou, R.; Shao, Y.; Wang, D.; Engelhard, M. H.; Kwak, J. H.; Wang, J.; Viswanathan, V. V.; Wang, C.; Lin, Y.; Wang, Y.; *et al.* Enhanced Activity and Stability of Pt Catalysts on Functionalized Graphene Sheets for Electrocatalytic Oxygen Reduction. *Electrochem. Commun.* **2009**, *11*, 954–957.
16. Yoo, E.; Okata, T.; Akita, T.; Kohyama, M.; Nakamura, J.; Honma, I. Enhanced Electrocatalytic Activity of Pt Subnanoclusters on Graphene Nanosheet Surface. *Nano Lett.* **2009**, *9*, 2255–2259.
17. Shao, Y. Y.; Zhang, S.; Wang, C. M.; Nie, Z. M.; Liu, J.; Wang, Y.; Lin, Y. H. Highly Durable Graphene Nanoplatelets Supported Pt Nanocatalysts for Oxygen Reduction. *J. Power Sources* **2010**, *195*, 4600–4605.
18. Choi, S. M.; Seo, M. H.; Kim, H. J.; Kim, W. B. Synthesis of Surface-Functionalized Graphene Nanosheets with High Pt-Loadings and Their Applications to Methanol Electrooxidation. *Carbon* **2011**, *49*, 904–909.
19. Zhang, B.; Zhang, C. B.; He, H.; Yu, Y. B.; Wang, L. A.; Zhang, J. Electrochemical Synthesis of Catalytically Active Ru/RuO_2 Core−Shell Nanoparticles without Stabilizer. *Chem. Mater.* **2010**, *22*, 4056–4061.
20. Rolison, D. R.; Hagans, P. L.; Swider, K. E.; Long, J. W. Role of Hydrous Ruthenium Oxide in Pt-Ru Direct Methanol Fuel Cell Anode Electrocatalysts: The Importance of Mixed Electron/Proton Conductivity. *Langmuir* **1999**, *15*, 774–779.
21. Li, F.; Chen, J.; Zhang, Q.; Wang, Y. Hydrous Ruthenium Oxide Supported on Co_3O_4 as Efficient Catalyst for Aerobic Oxidation of Amines. *Green Chem.* **2008**, *10*, 553–562.
22. Wendt, S.; Seitsonen, A. P.; Over, H. Catalytic Activity of RuO_2(110) in the Oxidation of CO. *Catal. Today* **2003**, *85*, 167–175.
23. Kim, Y. D.; Over, H.; Krabbes, G.; Ertl, G. Identification of RuO_2 as the Active Phase in CO Oxidation on Oxygen-Rich Ruthenium Surfaces. *Top. Catal.* **2001**, *14*, 95–100.
24. Walter, M. G.; Warren, E. L.; McKone, J. R.; Boettcher, S. W.; Mi, Q. X.; Santori, E. A.; Lewis, N. S. Solar Water Splitting Cells. *Chem. Rev.* **2010**, *110*, 6446–6473.
25. Song, S.; Zhang, H.; Ma, X.; Shao, Z.; Baker, R. T.; Yi, B. Electrochemical Investigation of Electrocatalysts for the Oxygen Evolution Reaction in PEM Water Electrolyzers. *Int. J. Hydrogen Energy* **2008**, *33*, 4955–4961.
26. Lewerenz, H. J.; Stucki, S.; Kotz, R. Oxygen Evolution and Corrosion—XPS Investigation on Ru and RuO_2 Electrodes. *Surf. Sci.* **1983**, *126*, 463–468.
27. Fang, Y.-H.; Liu, Z.-P. Mechanism and Tafel Lines of Electrooxidation of Water to Oxygen on RuO_2(110). *J. Am. Chem. Soc.* **2010**, *132*, 18214–18222.
28. Lyons, M. E. G.; Floquet, S. Mechanism of Oxygen Reactions at Porous Oxide Electrodes. Part 2: Oxygen Evolution at RuO_2, IrO_2 and $Ir_xRu_{1-x}O_2$ Electrodes in Aqueous Acid and Alkaline Solution. *Phys. Chem. Chem. Phys.* **2011**, *13*, 5314–5335.
29. Harding, J. R.; Lu, Y. C.; Tsukada, Y.; Shao-Horn, Y. Evidence of Catalyzed Oxidation of Li_2O_2 for Rechargeable Li-Air Battery Applications. *Phys. Chem. Chem. Phys.* **2012**, *14*, 10540–10546.
30. Wohlfahrtmehrens, M.; Heitbaum, J. Oxygen Evolution on Ru and RuO_2 Eletrodes Studied Using Isotope Labeling and Online Mass-Spectrometry. *J. Electroanal. Chem.* **1987**, *237*, 251–260.
31. Rossmeisl, J.; Qu, Z. W.; Zhu, H.; Kroes, G. J.; Norskov, J. K. Electrolysis of Water on Oxide Surfaces. *J. Electroanal. Chem.* **2007**, *607*, 83–89.
32. Lee, Y.; Suntivich, J.; May, K. J.; Perry, E. E.; Shao-Horn, Y. Synthesis and Activities of Rutile IrO_2 and RuO_2 Nanoparticles for Oxygen Evolution in Acid and Alkaline Solutions. *J. Phys. Chem. Lett.* **2012**, *3*, 399–404.
33. Oh, S. H.; Nazar, L. F. Oxide Catalysts for Rechargeable High-Capacity Li-O_2 Batteries. *Adv. Energy Mater.* **2012**, *2*, 903–910.
34. Chen, H.; Muller, M. B.; Gilmore, K. J.; Wallace, G. G.; Li, D. Mechanically Strong, Electrically Conductive, and Biocompatible Graphene Paper. *Adv. Mater.* **2008**, *20*, 3557–3561.
35. Wang, Z. L.; Xu, D.; Xu, J. J.; Zhang, L. L.; Zhang, X. B. Graphene Oxide Gel-Derived, Free-Standing, Hierarchically Porous Carbon for High-Capacity and High-Rate Rechargeable Li-O_2 Batteries. *Adv. Funct. Mater.* **2012**, *22*, 3699–3705.
36. Sun, B.; Wang, B.; Su, D. W.; Xiao, L. D.; Ahn, H.; Wang, G. X. Graphene Nanosheets as Cathode Catalysts for Lithium-Air Batteries with an Enhanced Electrochemical Performance. *Carbon* **2012**, *50*, 727–733.
37. McCloskey, B. D.; Bethune, D. S.; Shelby, R. M.; Girishkumar, G.; Luntz, A. C. Solvents' Critical Role in Nonaqueous Lithium-Oxygen Battery Electrochemistry. *J. Phys. Chem. Lett.* **2011**, *2*, 1161–1166.
38. Oh, S. H.; Black, R.; Pomerantseva, E.; Lee, J.-H.; Nazar, L. F. Synthesis of a Metallic Mesoporous Pyrochlore as a Catalyst for Lithium−O_2 Batteries. *Nat. Chem.* **2012**, *4*, 1004–1010.
39. Hassoun, J.; Croce, F.; Armand, M.; Scrosati, B. Investigation of the O_2 Electrochemistry in a Polymer Electrolyte Solid-State Cell. *Angew. Chem., Int. Ed.* **2011**, *50*, 2999–3002.
40. Jeong, Y. S.; Jung, H.-G.; Park, J.-B.; Sun, Y.-K.; Lee, Y. J. A Study on the Catalytic Activity of Noble Metal Nanoparticles on Reduced Graphene Oxide for Oxygen Evolution Reactions in Lithium-Air Batteries. Manuscript in preparation.
41. Rossmeisl, J.; Logadottir, A.; Norskov, J. K. Electrolysis of Water on (Oxidized) Metal Surfaces. *Chem. Phys.* **2005**, *319*, 178–184.
42. Peng, Z.; Freunberger, S. A.; Hardwick, L. J.; Chen, Y.; Giordani, V.; Barde, F.; Novak, P.; Graham, D.; Tarascon, J.-M.; Bruce, P. G. Oxygen Reactions in a Non-aqueous Li^+ Electrolyte. *Angew. Chem., Int. Ed.* **2011**, *50*, 6351–6355.
43. Hummers, W. S.; Offeman, R. E. Preparation of Graphitic Oxide. *J. Am. Chem. Soc.* **1958**, *80*, 1339–1339.
44. Xu, Y.; Sheng, K.; Li, C.; Shi, G. Self-Assembled Graphene Hydrogel *via* a One-Step Hydrothermal Process. *ACS Nano* **2010**, *4*, 4324–4330.
45. Ha, H.-W.; Kim, I. Y.; Hwang, S.-J.; Ruoff, R. S. One-Pot Synthesis of Platinum Nanoparticles Embedded on Reduced Graphene Oxide for Oxygen Reduction in Methanol Fuel Cells. *Electrochem. Solid State Lett.* **2011**, *14*, B70–B73.
46. Chang, K. H.; Hu, C. C. Hydrothermal Synthesis of Hydrous Crystalline RuO_2 Nanoparticles for Supercapacitors. *Electrochem. Solid State Lett.* **2004**, *7*, A466–A469.
47. Chen, Y.; Zhang, X.; Zhang, D.; Ma, Y. One-Pot Hydrothermal Synthesis of Ruthenium Oxide Nanodots on Reduced Graphene Oxide Sheets for Supercapacitors. *J. Alloys Compd.* **2012**, *511*, 251–256.